Organic Process Research & Development

ARTICLE

pubs.acs.org/OPRD

Rapid Determination of Reaction Kinetics with an Automated Microfluidic System

Jonathan P. McMullen and Klavs F. Jensen*

Department of Chemical Engineering, Novartis-MIT Center for Continuous Manufacturing, Massachusetts Institute of Technology, Cambridge, Massachusetts 02139, United States

Supporting Information

ABSTRACT: Kinetic information is used to determine the optimal reaction conditions, to successfully scale up a reaction from the laboratory to the pilot plant, and to improve process control. Obtaining accurate kinetics using conventional benchtop equipment and techniques, however, requires numerous experiments and can be complicated by sluggish mixing and heat-transfer rates. To improve the speed and efficiency in gathering reaction kinetics, we present an automated, silicon microreactor system that uses a sequential experimentation framework driven by model-based optimization feedback for online reaction rate parameter determination. The method, based on Information Theory and Bayesian Statistics, first selects the appropriate global reaction rate expression. After determining the correct rate law, a D-optimal strategy precisely estimates the pre-exponential and activation energy of the rate constant. The approaches are validated experimentally with a model system, the Diels−Alder reaction of isoprene and maleic anhydride in DMF. The benefits of quickly obtaining this information with an automated microreactor system are further demonstrated by successfully scaling the Diels−Alder reaction by a factor of 500 from a microreactor to a Corning flow reactor.

INTRODUCTION

Components of process development, such as reaction optimization and establishing the appropriate process control schemes, are greatly facilitated with the insight of the reaction kinetics. Obtaining accurate reaction rate parameters in conventional laboratory bench-scale equipment can be limited by several factors. In the pharmaceutical and fine chemical industries where reaction material can be minimal, insufficient data and improper experimental designs do not provide adequate information for reaction modeling. In situ analytical techniques, such as infrared spectroscopy and calorimetry, can be incorporated in batch reactors to increase the information content per experiment. However, concentration and temperature gradients that exist in these systems could provide misleading reaction results when assuming an ideal batch reactor kinetic model. This error is exacerbated for reactions that involve volatile reagents or reactions performed under reflux because the concentrations in solution and in the headspace are often unknown.[1] These limitations, however, are not a concern in microflow reactors, 'microreactors'. In addition to improving the accuracy of kinetic investigations, the enhanced heat- and mass-transfer rates in microreactors enables one to explore syntheses that are not easily studied in benchtop batch reactors, such as reactions that are extremely fast,[2] reactions that involve an unstable intermediate[3] or a highly toxic compound,[4] and reactions that show improved operations at high temperature and pressures.[5] Further efficiency is gained by combining the continuous-flow operations of microreactors with inline analysis and feedback control to automate the experiments involved in the kinetic investigation.

The benefits of automated microreactor systems have been demonstrated for a variety of reaction development applications.[6−11] We have previously described an automated microreactor system capable of online, multiparameter reaction optimization as well as the ability to transfer these results from the micro- to the mesoscale.[12,13] Black-box optimization algorithms were implemented in these studies, enabling rapid reaction optimization while requiring little knowledge of the reaction system. These approaches are ideal when the goal of the experiments is to evaluate a specific reaction metric, such as maximizing the product yield, and then scaling up to a plug flow reactor (PFR). While this information is a vital component of process development, the application of the experimental results may be limited if the objective should later change, say to maximize product purity instead of yield, or if the process is scaled up to a reactor other than a traditional PFR. To avoid these restrictions, a more information-enriched approach could be used to quickly and efficiently obtain intrinsic reaction knowledge. In the present work, we demonstrate this concept by implementing two model-based optimization feedback algorithms within an automated microreactor system to ascertain the kinetics of a Diels−Alder reaction and scale up the reaction by a factor 500.

Reaction rate modeling includes two aspects—determining the reaction rate form and estimating the parameters of the rate constants (pre-exponential and activation energy). Common procedures to extract this information are outlined in kinetics and chemical engineering textbooks.[14,15] First a global rate expression, such as a common power law or complex rate form is assumed. Numerous investigative experiments are performed, and the data is collected and analyzed to determine the reaction order and rate constant parameters. Great advances in high throughput technology and parallel experimentation have significantly decreased the amount of time required to acquire the

Received: November 9, 2010
Published: March 04, 2011

data,[16,17] but the amount of useful information gained per experiment could be low. For example, when considering the experimental variance and the sensitivity of a rate model to the fitted parameters, different rate law models can appear to adequately fit the data over a range of experimental conditions. Therefore, the results from these investigative experiments cannot be used to statistically distinguish the form or the order of the reaction rate. Even when the rate law is known, these experiments may not be useful for precisely estimating the pre-exponential and the activation energy because the statistical significance of these estimates is highly dependent upon the experimental design. A superior approach to kinetic modeling is to perform an experiment, analyze the results, use the data to discriminate between various rate models and to estimate kinetic parameters, and apply an appropriate algorithm to select sequential experiments that will maximize the reaction information. Although this sequential procedure would be slow and laborious for batch experimentation, this approach is straightforward when using automated microreactor systems with inline analysis.

A variety of sequential experimental designs have been proposed to determine the global reaction rate model. From a library of potential rate laws, these techniques continue to perform experiments until one model has proven to best describe the data. We implemented a framework developed by Box and Hill that uses Information Theory and Bayesian Statistics to discriminate among the most likely rate models that describe experimental observations.[18] A general description of this technique follows, while a more detailed discussion of the algorithm and the necessary equations are provided in the Supporting Information. In this approach, each rate model has a probability of correctly predicting experimental outcome as defined by eq 1, where p_i is the probability function of rate law model i, y_N is the Nth experimental observation (i.e., yield), $\hat{y}_N^i$ is the experimental outcome predicted by model i, σ_i^2 is the variance of model i, σ^2 is the experimental variance, and $\mathbf{x}$ is the vector of experimental conditions (i.e., temperature, residence time, concentrations).

$$p_i(\mathbf{x}) = \frac{1}{\sqrt{2\pi(\sigma^2(\mathbf{x}) + \sigma_i^2(\mathbf{x}))}} \exp\left\{ -\frac{(y_N(\mathbf{x}) - \hat{y}_N^i(\mathbf{x}))^2}{2(\sigma^2(\mathbf{x}) + \sigma_i^2(\mathbf{x}))} \right\} \tag{1}$$

From Information Theory, the ability of a particular rate expression to predict experimental observations more adequately than all potential models is related to Shannon's Entropy. Initially, before any experimental data is obtained, there is no information to determine which model describes the reaction rate; therefore, Shannon's Entropy is at a maximum value. After obtaining adequate experimental data, one model has a higher probability of describing the reaction rate over the other models, corresponding to a less entropic state. The design by Box and Hill aims at selecting sequential experiments where the change in Shannon's Entropy is expected to be a maximum. This maximum expected change in Shannon's Entropy for any set of experimental conditions, denoted as $D(\mathbf{x})$, is given by eq 2, where i and j are indices for the M potential rate models, and Π_{N-1} is the Bayesian prior probability. Sequential experimentation continues until the Bayesian posterior probability, a metric used to assess a model's capabilities to describe the experimental observations, surpasses a specified threshold.

$$D(\mathbf{x}) = \frac{1}{2} \sum_{i=1}^{M-1} \sum_{j=i+1}^{M} \Pi_{i,N-1} \Pi_{i,N-1} \left\{ \frac{(\sigma_i^2(\mathbf{x}) - \sigma_j^2(\mathbf{x}))^2}{(\sigma^2(\mathbf{x}) + \sigma_i^2(\mathbf{x}))(\sigma^2(\mathbf{x}) + \sigma_j^2(\mathbf{x}))} + (\hat{y}_N^i(\mathbf{x}) - \hat{y}_N^j(\mathbf{x}))^2 \left(\frac{1}{(\sigma^2(\mathbf{x}) + \sigma_i^2(\mathbf{x}))} + \frac{1}{(\sigma^2(\mathbf{x}) + \sigma_j^2(\mathbf{x}))} \right) \right\} \tag{2}$$

The method by Box and Hill was implemented in this work because the Bayesian approach considers previous information and parametric uncertainty to discriminate models in few experiments. The ability to determine the correct rate law with a minimal number of experiments is important for modeling pharmaceutical and fine chemical reactions because the availability of reagents or catalysts can be limiting. However, significant advances in the robustness and efficiency in other model discrimination algorithms have been established over the years.[19−23] Selection of the most appropriate criterion for model discrimination approaches has been a primary focus,[24,25] as well as extending these techniques to multiresponse models.[26−29] To demonstrate the usefulness of these algorithms, computer simulations have been performed to demonstrate the improvements to reaction modeling for a myriad of applications.[30−36] Incorporation of these techniques with experimental data are less reported, but applications include hydrogenation[37] and crystallization.[38] The experimental designs in these applications were developed before data collection. Imbedding a feedback mechanism to perform experiments, collect data, and update the sequential experimental design offers a great improvement to the speed and efficiency for model discrimination applications.

After the appropriate rate law is determined, additional experiments are performed to refine the rate constant parameters. Computing precise values for pre-exponential and activation energy is a challenging task because of the high correlation. Additionally, the precision of these estimates is highly dependent upon experimental design, indicating that some experimental conditions provide more information content than others. Even if ample experiments are performed in a kinetic investigation, such as the scenario of running parallel experiments in 96-well plates, the precision in the kinetic values will be poor if the appropriate experimental conditions were not selected. The relationship between the experimental design and the precision in parameter estimates is apparent in the definition of the joint confidence region, c, around the set of best fit parameters, θ^*,[39]

$$(\theta - \theta^*)^T \mathbf{M}_f (\theta - \theta^*) = c \tag{3}$$

$$\mathbf{M}_f(\theta, \mathbf{x}) = \sum_{i=1}^{N-1} \left(\left[\frac{\partial y(\theta, x_i)}{\partial \theta} \right]^T \Sigma^{-1} \left[\frac{\partial y(\theta, x_i)}{\partial \theta} \right] \right) \tag{4}$$

where c is a constant given by the F-distribution and Σ^{-1} is the experimental variance matrix.

As shown in eq 3, the volume of this joint confidence region is proportional to a matrix, $\mathbf{M}_f$, known as the Fisher Information matrix, which is also the inverse of the parameter variance−covariance matrix.[21] Optimal experimental designs, such as A-, D-, E-, and G-optimal designs, use various properties associated with $\mathbf{M}_f$ to select experiments aimed at maximizing parameter

Scheme 1. Diels−Alder reaction of isoprene with maleic anhydride to form

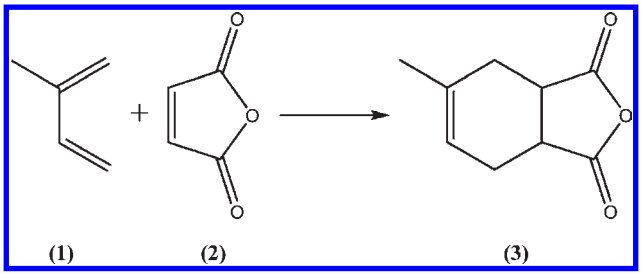

estimate precision.[21] Benefits of these designs have been demonstrated for various process chemical fields, including chemical kinetics,[39] biokinetics,[40] crystallization,[41] and heat- and mass transfer.[42] Perhaps the most common approach, D-optimal, is used in this work for kinetic parameter estimation. After performing $N-1$ experiments, the D-optimal criterion selects the Nth experiment by determining the conditions that minimize the volume of the joint confidence region. Mathematically, these conditions correspond to the experiment that maximizes the determinant of the inverse of $\mathbf{M_f}$ (eq 5).

$$\mathbf{x}_N = \arg\min |\mathbf{M}_f^{-1}| \quad (5)$$

By continuously updating the Fisher Information matrix with each new experiment, and sequentially selecting experiments according to eq 5, precise kinetic parameters can be calculated in a minimal number of experiments.

The approaches discussed above were implemented in an automated microreactor system and experimentally tested with the Diels−Alder reaction of isoprene and maleic anhydride in DMF (Scheme 1). This model reaction was selected because it is straightforward, there are no observed side reactions at the temperatures that were investigated, and the kinetics have been well-established in previous studies.[43,44] Therefore, the results from this investigation are used to validate the operations of the automated microreactor system as well as to demonstrate the speed and the efficiency in using model-based approaches to experimentally obtain kinetics. In the first part of this investigation, model discrimination techniques are applied to select the rate law model that correctly describes the consumption of isoprene (eq 6) from the list of possible rate laws given by eqs 6-9. In these rate expressions, r_i is the rate of isoprene consumption as represented by rate expression i, k_i is the corresponding rate constant for expression i, and C_1 and C_2 denote the concentration of isoprene and maleic anhydride, respectively. After selecting the most likely reaction model, the automated system performed sequential experiments using a D-optimal design to determine the rate constant parameters.

$$r_{\mathrm{I}} = -k_{\mathrm{I}} C_1 C_2 \quad (6)$$

$$r_{\mathrm{II}} = -k_{\mathrm{II}} C_1^2 C_2 \quad (7)$$

$$r_{\mathrm{III}} = -k_{\mathrm{III}} C_1 C_2^2 \quad (8)$$

$$r_{\mathrm{IV}} = -k_{\mathrm{IV},f} C_1 C_2 + k_{\mathrm{IV},r} C_3 \quad (9)$$

EXPERIMENTAL METHODS

Microreactor System. A schematic of the automated system used in these investigations is illustrated in Figure 1. Standard photolithography and deep reactive ion etching techniques were used to create a 120 μL reactor with 400 μm × 400 μm channel dimensions. A spiral reactor design was used so that this system could be used for future kinetics studies of reactions that involve solids byproducts, such as palladium coupling reactions.[45] A compression packaging scheme was used to make fluidic connections between the microreactor and macrofluidic instruments. The residence time and the reagent concentrations were adjusted by varying the flow rates of the syringe pumps. A halo etch was incorporated in the microreactor design, enabling the device to operate at two different temperature zones. The temperature of the mixing and outlet zones was controlled by pumping 20 °C water through the fluidic chuck using a circulating bath, while the reaction zone was heated using a thermoelectric module. By cooling the reaction to 20 °C, the Diels−Alder reaction was effectively quenched. The reaction stream was immediately diluted off-chip by a factor of 5, and an interdigital micromixer was used to ensure rapid mixing before inline HPLC analysis.[3] Although inline spectroscopic techniques such as Raman[46] and ATR-IR[47] have been incorporated with microfluidic systems, an HPLC was integrated into the microfluidic system because this analytical method provides multicomponent information and can be used to quantify a wider range of reaction types than inline spectroscopy alone. An isocratic HPLC method using 1:1 water/acetonitrile at 1.5 mL/min was used for analysis. Reaction model discrimination and parameter estimation was performed by monitoring the outlet concentration of isoprene. This concentration was determined by using a response factor and the ratio of the isoprene chromatogram at 247 nm to the chromatogram of the internal standard, biphenyl, at 280 nm. Further details of the system components and automation procedure are given in the Supporting Information.

Because the reaction results were not expected to be influenced by the ±1 °C tolerance in the temperature control or slight oscillations in the syringe pump, the experimental variance was assumed to be that of the HPLC measurement variance and constant. A calibration curve for isoprene with repeat concentration points was created in an automated manner by using three syringe pumps and the micromixer.[12] By loading a concentrated solution of isoprene in one syringe, biphenyl in the second, and DMF in the third to act as diluent, a calibration curve for isoprene and biphenyl was created over a range of concentrations. Conducting these calibrations at various flow rates verified that there was no correlation between HPLC measurement and the syringe pump performance.

KINETIC MODELING APPROACHES ON THE MICRO- AND MESOSCALES

Online Model Discrimination. Using the model discrimination algorithm described above, the automated microreactor system selected and performed experiments to determine the correct rate law from the potential models given by eqs 6−9. The manipulated variables during this investigation were residence time and the reactor inlet concentrations of **1** and **2**. To obtain an initial estimate for the rate constants in each model, a preliminary set of experiments were performed corresponding to a half-

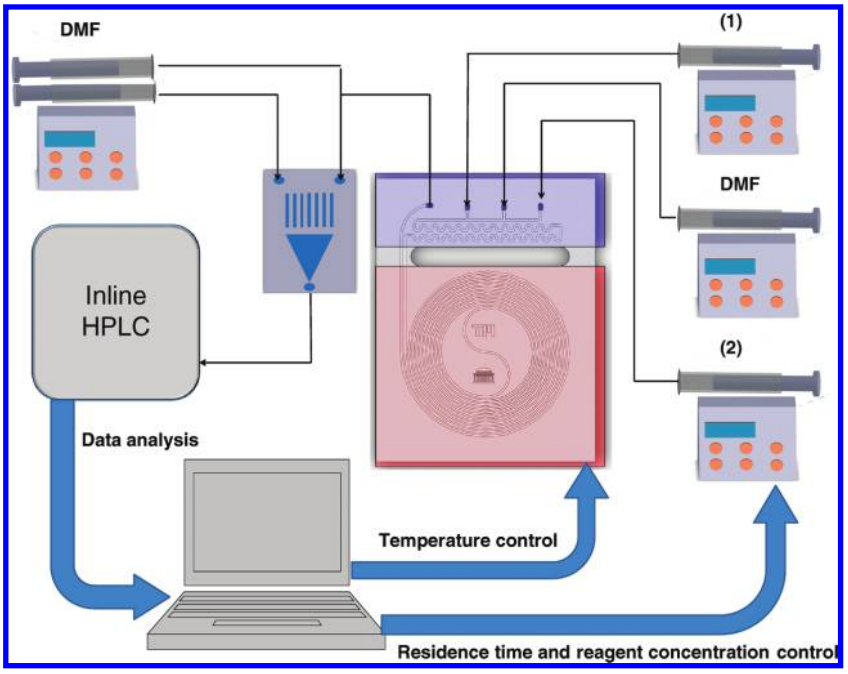

Figure 1. Sketch of automated microreactor system for online model discrimination and parameter estimation. The red-shaded zone of the microreactor indicates the reaction zone, and the portion of the reactor maintained at 20 °C is denoted by the blue shaded area. The high thermal conductivity of silicon and the small reactor channel width ensures that the reaction mixture is cooled before exiting the microreactor, thereby quenching this Diels−Alder reaction.

fractional factorial.[48] Rate constants were estimated by minimizing the sum of squared errors. Computationally, this estimation was achieved in Matlab using a nonlinear optimization solver (fmincon) using the active-set algorithm for models r_I−r_{III} and the interior-point algorithm for model r_{IV}. The model responses, predictions, and sensitivities were estimated using a PFR model for each rate model and a differential equation solver (ode15s). As will be discussed later, a PFR model is appropriate over the range of experimental conditions that were investigated. After these four preliminary experiments, sequential experiments used the previous rate constant solution as the initial guess.

Once the preliminary experiments were performed and the best-fit rate constants and the model variances were computed, the fifth and subsequent experiments were determined by finding the conditions that maximized D of eq 2. Because the isoprene outlet concentration was modeled by numerically solving the differential rate equations, determining the global minimum of D using nonlinear optimization solvers was deemed too computationally expensive for the solution purpose and problem size. Instead, the parameter space was discretized to grid points defined by residence times between 1 and 10 min in intervals of 0.5 min and **1** and **2** inlet concentrations between 0.5 and 2.0 M in increments of 0.25 M. Values of D were explicitly enumerated, and the sequential experiments were determined by locating the grid point with the maximum D value. Experimentation continued until the Bayesian posterior probability of rate model surpassed 95%, or if it was determined that discrimination could no longer be achieved.

Online Parameter Estimation. After determining the correct rate law, the automated microreactor system was used to estimate the pre-exponential and the activation energy parameters of the rate constant. Similar to the model discrimination investigation, the isoprene reactor outlet concentration was modeled with PFR kinetics. However, the laminar flow in microfluidics creates a parabolic velocity profile that results in axial dispersion.[49] The degree of dispersion and the discrepancy between the PFR and the laminar flow reactor kinetic models is dependent upon the experimental conditions. To avoid the complications of modeling the reaction environment as a laminar flow reactor, computer simulations were performed to determine a range of experimental conditions where the effects of dispersion would be minimal and where modeling the reaction with PFR kinetics would be satisfactory. This approach and the simulated results are located in the Supporting Information. The results indicated that an appropriate design space for this kinetic study was the region bounded by 50−150 °C and residence times between 1 and 10 min.

Experiments for parameter estimation followed the D-optimal design framework and used temperature and residence time as variables. The design space was discretized to form a grid of potential experiments, corresponding to temperatures between 50° and 150 °C in increments of 10 °C and residence times between 1 and 10 min in intervals of 0.5 min. The reactor inlet concentrations of **1** and **2** remained constant during these experiments at 1.0 M. Four preliminary experiments corresponding to a full factorial were performed to arrive at initial estimates for the pre-exponential and activation energy. Parameter estimation was performed by minimizing the sum of squared errors with a nonlinear optimization solver in Matlab. The estimates were substituted into the Fisher Information matrix (see eq 4) and sequential experiments were selected by locating the experimental point that satisfied eq 5. Sequential experimentation continued until the activation energy estimate (E_a) and 95% confidence intervals (ΔE_a) converged according to eqs 10 and 11. This confidence interval provides the upper and lower bounds on the values for E_a in the joint confidence region described by eq 3. Although developing termination criteria based on the actual joint confidence region could provide more insight to the parameter estimates, the 95% confidence intervals are

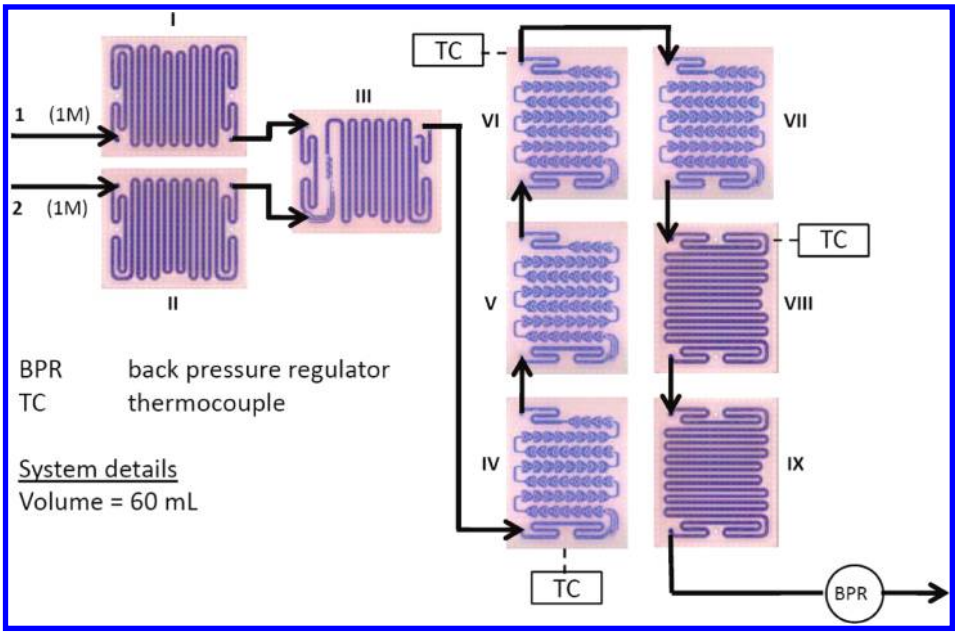

Figure 2. Illustration of Corning AFR system used to scale up reaction by a factor of 500. AFR modules are denoted by Roman numerals I−IX. AFR modules I and II are used to heat the individual reagent streams to the desired reaction temperature. Reagent streams combine and are mixed via a static mixer in module III. The reaction proceeds in modules III−IX, and samples are quenched and collected at the system outlet.

significantly faster to compute and therefore more attractive to implement in an automated system.

$$\frac{|E_{a_N} - E_{a_{N-1}}|}{E_{a_N}} \leq 5\% \tag{10}$$

$$\frac{|\Delta E_{a_N} - \Delta E_{a_{N-1}}|}{\Delta E_{a_N}} < 10\% \tag{11}$$

Application of Kinetic Results to Scale Up. Difficulty in scaling from the test tube to the pilot is due to the complexity of the mixing and heat transfer in batch systems. Flow systems, on the other hand, have been studied and characterized for over a century due to their dominant presence in the petroleum and commodity chemical industries. To demonstrate the benefits of using kinetic information quickly obtained with automated microreactor systems, we scaled up the Diels−Alder reaction to a 60 mL Advanced Flow Reactor System (AFR) by Corning. This scale up corresponds to a factor of 500. Our goal was to predict the conversion of isoprene at several different conditions in the AFR system.

A schematic of the AFR system for scale up is shown in Figure 2. A high-pressure Isco pump and a Fuji Super Metering pump were used to deliver maleic anhydride and isoprene, respectively. Two plates were used to preheat the reagents to the reaction temperature before entering the first reaction plate. A static mixer in the first reactor plate was used to create a uniform mixture. Previous reports indicate that mixing in these devices is sufficient for flow rates above 15 mL/min for each reagent.[50] Reaction temperature was controlled by pumping Kryo 55 oil with a Lauda circulating bath through the two 18-channel heat exchangers that cap the reaction channel. Reaction temperature was monitored by thermocouples that were inserted into the heat exchanger fluid lines. An adjustable back pressure regulator was added to the outlet to prevent solvent degassing during reaction. Reaction samples were taken by collecting approximately 20 mL of the reaction outlet stream into 80 mL of DMF that was kept at 0 °C. This collection arrangement effectively quenched the reaction. Samples were stored at 0 °C until analyzed by HPLC.

Successful scale up of flow systems uses the reaction kinetics, the heat-transfer rates, and the residence time distribution (RTD) to solve the material and energy balances of the reaction. This approach is especially important for exothermic reactions, such as this Diels−Alder example, which has a large heat of reaction, $\Delta H_{rxn} \approx -145$ kJ/mol.[44] Although experimental measurements of the heat transfer and the RTD of the entire AFR system provides the most accurate information for scale up, excellent approximations for these features are obtained through simple characterization experiments and general correlations. A dispersion model, $E(t)$ as given by eq 12, was used to estimate the residence time distribution and the dispersion coefficient, $\mathbf{D}^*$, was experimentally measured by recording the tracer curve for a pulse injection through a single AFR plate reactor.[15] In this equation, L is the length of the reactor and U is the average fluid velocity. The heat-transfer rate, Q, was estimated by calculating the overall heat-transfer coefficient for an AFR plate, U_{HX}, which has been previously reported for several flow conditions.[51] Over the range of conditions investigated in this work, the values of the overall heat transfer coefficient ranged from 180 to 360 W/m^{2}K. The heat-transfer rate is used to solve the energy balance of the reaction system and to estimate the temperature rise caused by the exothermic reaction. Further details of the modeling and simplifying assumptions are given in the Supporting Information. This heat transfer information is used to solve the coupled mass (eq 14) and energy (eq 15) balances, where P_{HX} and A_{CS} is the perimeter and the cross-sectional area of the heat transfer area, respectively. The isoprene concentration exiting the AFR system is calculated by incorporating the solution from these equations into the RTD

Table 1. Experimental results, algorithm parameter *D* (see eq 2), and posterior probabilities associated with model discrimination experiments

				.		posterior probability			
exp	residence time (min)	**1** (M)	**2** (M)	conversion	D	Π_{I}	Π_{II}	Π_{III}	Π_{IV}
1	6.0	1.0	1.0	89	–	0.250	0.250	0.250	0.250
2	5.0	1.5	1.0	68	–	–	–	–	–
3	6.0	1.0	1.5	95	–	–	–	–	–
4	5.0	1.5	1.5	87	–	–	–	–	–
5	1.0	0.5	0.5	37	429000	0.470	0.356	0.173	<0.001
6	1.0	2.0	1.25	40	7.9	0.999	<0.001	<0.001	<0.001

Table 2. Rate constant estimates for each rate model considered in the kinetic discrimination investigation

model parameter estimate (see eqs 6−9)	after 4 experiments	after 5 experiments	after 6 experiments
$k_{I} \times 10^{2}$ (M^{-1} s^{-1})	1.69	1.74	1.34
$k_{II} \times 10^{2}$ (M^{-1} s^{-1})	6.63	5.95	1.95
$k_{III} \times 10^{2}$ (M^{-1} s^{-1})	8.88	6.90	3.15
$k_{IV,f} \times 10^{2}$ (M^{-1} s^{-1})	13.4	2.08	1.34
$k_{IV,r} \times 10^{3}$ (s^{-1})	2.56	0.21	0.00

model (eq 16).

$$E(t) = \frac{U}{\sqrt{4\pi \mathbf{D}^{*} t}} \exp\left(-\frac{(L-Ut)^{2}}{4\mathbf{D}^{*} t}\right) \tag{12}$$

$$Q = U_{HX} A_{HX} (T_{rxn} - T_{oil}) \tag{13}$$

$$\frac{dC_{1}}{dt} = -kC_{1}^{2} \tag{14}$$

$$\rho C_{P} \frac{dT}{dt} = \frac{U_{HX} P_{HX}}{A_{CS}} (T - T_{oil}) - kC_{1}^{2} \Delta H_{rxn} \tag{15}$$

$$\overline{C}_{1} = \int_{t=0}^{\infty} C_{1}(t) E(t) dt \tag{16}$$

RESULTS AND DISCUSSION

The first component of this kinetic investigation involved determining the correct rate law expression that described the consumption of isoprene. Results from this model discrimination investigation are listed in Table 1. Initially, each reaction model was assumed to be equally as likely to be the correct rate law; therefore, the prior probability was 0.25 for each model. After performing the preliminary experiments (exp 1−4), rate constants for each model were fitted and are listed in Table 2. The kinetic values for each rate model were used to select the fifth experiment by finding the conditions that maximized the value of *D* (eq 2). These conditions corresponded to a residence time of 1 min and 0.5 M reactor inlet concentrations for both **1** and **2**. As previously mentioned, each reaction model has a probability distribution that describes the likely experimental outcome at these conditions (eq 1). These distributions for the reactor outlet concentration of isoprene for the fifth experiment are shown in Figure 3, along with the experimental outcome.

Upon inspection of Figure 3, one will notice that the probability distribution for model r_{IV} appears to be missing. This apparent omission is related to the best-fit estimates that were computed for model r_{IV} from the first four experiments. The nonzero value for the reverse rate constant, $k_{IV,r}$, provides a better fit to the initial data set than that of a model that does not include a reverse reaction. Although the combination of rate constant estimates for model r_{IV} resulted in a better fit to the first four experiments, the model prediction capabilities are quite sensitive to the value of the reverse rate constant. This type of sensitivity is common when a parameter estimate has no physical significance to a reaction model, but rather serves to minimize the residual error between the experimental data and reaction model estimates. Consequently, this high sensitivity translated into a high model variance for rate r_{IV}, and created a broad probability density function that cannot be seen on the same scale with the other rate law models in Figure 3.

Perhaps of greater interest is the product of these model probability functions with the corresponding Bayesian prior probabilities ($p_i \Pi_{i,N-1}$). This weighted probability function illustrates the ability of an experimental outcome to successfully discriminate the correct reaction model from other potential models. Discrimination is achieved when the experimental outcome falls within a single model weighted probability function. Because the prior probabilities for each model going into the fifth experiment were equal, this comparison can be made by simply looking at the individual model probabilities (Figure 3). Because the outcome of the fifth experiment falls within the prediction of several models, sequential experiments must be performed for discrimination.

The outcome for experiment 5 was used to calculate the posterior probability of each model. The posterior probability became the prior probability for the next experiment, and was used in the calculation of *D* to determine the conditions of experiment (exp) 6, corresponding to 1 min residence, 2.0 and 1.5 M reactor inlet concentrations of **1** and **2**, respectively. The weighted probability density function for the outlet isoprene concentration of exp 6 and the observed outcome are shown in Figure 4. As this figure indicates, the outcome from exp 6 was predicted only by reaction model r_{I}, implying that this model is the correct rate law. Mathematically, the posterior probabilities denoted that r_{I} was the correct rate law (see Table 1), and the experimental procedure was terminated. This prediction is in agreement with the known rate law for this reaction.[44] It is also interesting to note that reverse rate constant for model r_{IV} was zero when data from all six experiments were used in the

dx.doi.org/10.1021/op100300p |*Org. Process Res. Dev.* 2011, 15, 398–407

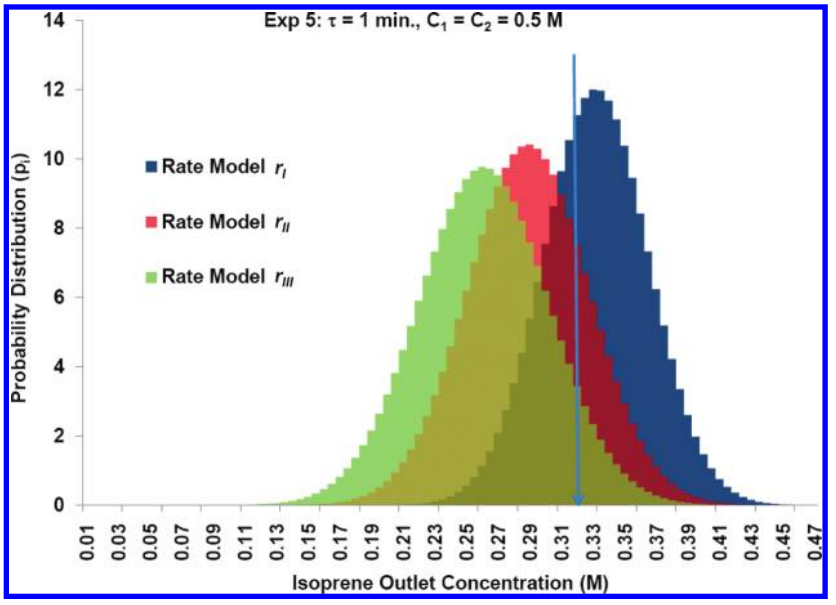

Figure 3. Probability distributions (p_i) of potential rate laws used for model discrimination calculations involved in selecting conditions for experiment 5. Experimental result is denoted by the arrow.

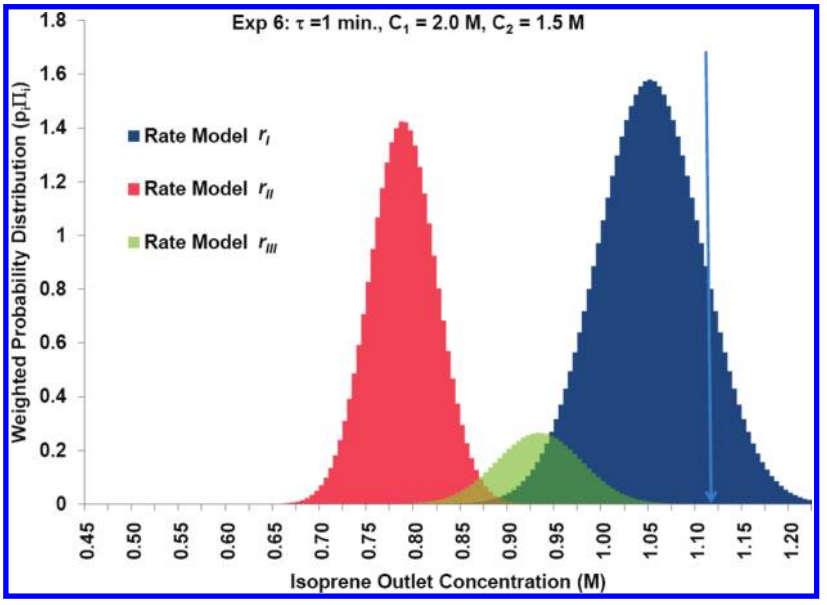

Figure 4. Weighted probability distributions ($p_i\Pi_i$) of potential rate laws used for model discrimination calculations involved in selecting conditions for experiment 6. Experimental result is denoted by the arrow.

nonlinear regression. This observation illustrates the caution that should be exercised when fitting parameters with few data points but also highlights the ability of this discrimination approach to avoid reaction models that contain unnecessary parameters.

Using the correct rate expression r_I from the model discrimination investigation, the microreactor system selected and performed experiments to estimate the kinetic parameters. Progression of the parameter estimation and the 95% confidence intervals for the sequential experiments are shown in Table 3. Using a D-optimal approach and the termination criteria given by eqs 10 and 11, precise estimates were achieved after six experiments. Observed values in this work are in good agreement with Hoffmann et al., who previously reported the activation energy for this Diels−Alder reaction as 58.5 ± 2 kJ/mol.[44]

These confidence intervals provide the upper and lower bounds for the parameter estimates, but of more importance is the joint confidence region (Figure 5), which captures the correlation between the parameters. Additionally, this information can be used to select the appropriate combinations of the pre-exponential factors and activation energies to determine the actual range for rate constant. For example, using the final best fit pre-exponential and activation energy, the rate constant at 100 °C is $(2.71 \pm 0.15) \times 10^{-2}$ M^{-1} s^{-1}. As an additional point of comparison, using the kinetic parameters reported by Hoffmann and co-workers provides a rate constant value of 2.6 ×

dx.doi.org/10.1021/op100300p |*Org. Process Res. Dev.* 2011, 15, 398–407

Table 3. Experimental for parameter estimation investigation with associated 95% confidence intervals[a]

					kinetic parameters	
exp	residence time (min)	temp (°C)	conversion	$\lvert M_f^{-1}\rvert \times 10^{30}$	$A \times 10^6$ M^{-1} s^{-1}	E_a kJ/mol
1	5.0	90	82		–	–
2	5.0	110	93		–	–
3	6.0	90	86		–	–
4	6.0	110	94	70.0	1.9 ± 10.5	56.1 ± 17.3
5	1.0	50	50	4.7	1.4 ± 1.0	55.3 ± 2.0
6	1.0	120	81	3.3	**2.1 ± 1.3**	**56.3 ± 1.9**

[a] The metric $\lvert M_f^{-1}\rvert$ (see eq 4) is provided for experiments 4−6 to provide some insight to the convergence of the algorithm.

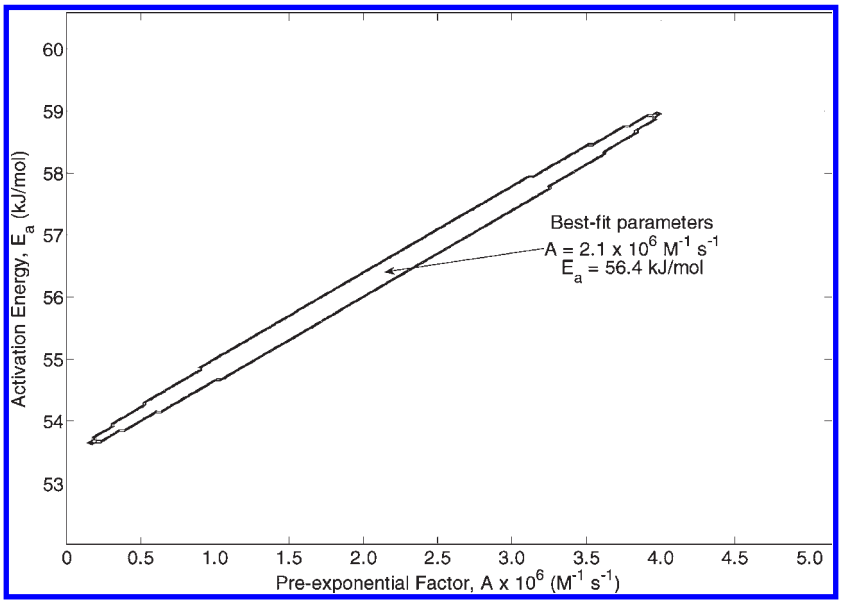

Figure 5. Joint confidence region for kinetic parameters determined by automated microreactor system.

Table 4. Predicted and experimental conversion for scale up investigation

				conversion	
entry	samples	time (min)	temp (°C)	experimental	predicted
1	2	1.5	110	78.1 ± 0.4	80.5
2	3	2.0	100	82.6 ± 0.1	84.7
3	3	2.5	110	85.2 ± 1.0	87.5
4	2	1.0	126	83.5 ± 3.1	84.8

10^{-2} M^{-1} s^{-1} at 100 °C, which falls within the range described by this joint confidence region.

The kinetic information obtained from the automated microreactor system was used with the RTD and heat transfer calculations to model the Diels−Alder reaction in the Corning AFR. For inlet reagent concentrations of 1.0 M each, model predictions at several experimental conditions were made by simultaneously solving the mass (eq 14) and energy (eq 15) balances and incorporating the solutions of these balances into the RTD model (eq 16) to determine the expected conversion of isoprene in the AFR reactor. Experimental results are compared to the scale up model predictions in Table 4, and are in excellent agreement with one another. The predicted conversion values are consistently higher than the observed experimental conversion. This trend is attributed to the underestimated value of the overall heat transfer coefficient (see Supporting Information), causing the exotherm predicted by the scale up model, which had a maximum value of +5 °C, to be larger than what would be observed experimentally. The strong influence of the heat transfer predictions underscores the need for having a well characterized system, such as the developed automated microreactor system, when determining reaction kinetics and predicting scale up performance.

■ CONCLUSIONS

An automated microreactor system combined with model-based optimization feedback has been presented as a technique to quickly model reactions while requiring a minimum number of experiments. Using less than five grams of each starting reagent in a Diels−Alder reaction, the microreactor system selected and performed 12 experiments to determine the appropriate rate law expression and to precisely estimate the pre-exponential and activation energy of the rate constant. This kinetic information was incorporated into a roadmap for continuous flow scale up, and validated by scaling the Diels−Alder reaction by a factor of 500 in a Corning AFR system. The experimental observations for this scale up were in good agreement with model predictions.

dx.doi.org/10.1021/op100300p |*Org. Process Res. Dev.* 2011, 15, 398–407

Current investigations with automated microfluidic systems involve obtaining the kinetics for syntheses that involve multiple reactions (i.e., parallel and serial reactions) that are more pharmaceutically relevant. In addition to the fast scale up of reactions, the intrinsic kinetic information gained from the microreactor system can be incorporated with advanced control schemes to ensure product quality during changes in production schedules. Modeling the different reactions rates using the tools and techniques demonstrated in this work will lead to fast and accurate reaction optimization results for complex chemical systems, such as those that involve multiple reactive pathways. Kinetic information for individual reactions will be extended to the design of optimal multistep processes. Furthermore, advances in in situ monitoring in microreactors will enable automated microreactor systems with model-based feedback to complement chemical computational techniques for reaction mechanism generation.

■ ASSOCIATED CONTENT

Supporting Information. Further details regarding the automated microreactor system components, operations, and experimental procedure, model discrimination approach, and numerical modeling of the scale up process. This material is available free of charge via the Internet at http://pubs.acs.org.

■ AUTHOR INFORMATION

Corresponding Author
kfjensen@mit.edu Fax: 1-617-258-8224 Tel: 1-617-253-4589

■ ACKNOWLEDGMENT

We thank Corning for generously providing an AFR system, Patrick Heider for RTD data of an AFR plate, and Novartis for financial support.

■ REFERENCES

(1) Bedore, M. W.; Zaborenko, N.; Jensen, K. F.; Jamison, T. F. *Org. Process Res. Dev.* **2010**, *14* (2), 432–440.
(2) Yoshida, J.-i.; Nagaki, A.; Yamada, T. *Chem.—Eur. J.* **2008**, *14* (25), 7450–7459.
(3) Zaborenko, N.; Murphy, E. R.; Kralj, J. G.; Jensen, K. F. *Ind. Eng. Chem. Res.* **2010**, *49* (9), 4132–4139.
(4) Zhang, X. N.; Stefanick, S.; Villani, F. J. *Org. Process Res. Dev.* **2004**, *8* (3), 455–460.
(5) Marre, S.; Park, J.; Rempel, J.; Guan, J.; Bawendi, M. G.; Jensen, K. F. *Adv. Mater.* **2008**, *20* (24), 4830–4834.
(6) Krishnadasan, S.; Brown, R. J. C.; deMello, A. J.; deMello, J. C. *Lab Chip* **2007**, *7* (11), 1434–1441.
(7) Sugimoto, A.; Fukuyama, T.; Rahman, M. T.; Ryu, I. *Tetrahedron Lett.* **2009**, *50* (46), 6364–6367.
(8) Garcia-Egido, E.; Spikmans, V.; Wong, S. Y. F.; Warrington, B. H. *Lab Chip* **2003**, *3* (2), 73–76.
(9) Goodell, J. R.; McMullen, J. P.; Zaborenko, N.; Maloney, J. R.; Ho, C.-X.; Jensen, K. F.; Porco, J. A.; Beeler, A. B. *J. Org. Chem.* **2009**, *74* (16), 6169–6180.
(10) Koch, K.; van Weerdenburg, B. J. A.; Verkade, J. M. M.; Nieuwland, P. J.; Rutjes, F. P. J. T.; van Hest, J. C. M. *Org. Process Res. Dev.* **2009**, *13* (5), 1003–1006.
(11) Nieuwland, P. J.; Koch, K.; van Harskamp, N.; Wehrens, R.; van Hest, J. C. M.; Rutjes, F. P. J. T. *Chem.—Asian J.* **2010**, *5* (4), 799–805.
(12) McMullen, J. P.; Jensen, K. F. *Org. Process Res. Dev.* **2010**, *14* (5), 1169–1176.
(13) McMullen, J. P.; Stone, M. T.; Buchwald, S. L.; Jensen, K. F. *Angew. Chem., Int. Ed.* **2010**, *49* (39), 7076–7080.
(14) Fogler, H. S., *Elements of Chemical Reaction Engineering*, 4th ed.; Prentice Hall: Upper Saddle River, NJ, 2006.
(15) Levenspiel, O. *Chemical Reaction Engineering*, 3rd ed.; Wiley: New York, 1999.
(16) Shultz, C. S.; Krska, S. W. *Acc. Chem. Res.* **2007**, *40* (12), 1320–1326.
(17) Rubin, A. E.; Tummala, S.; Both, D. A.; Wang, C.; Delaney, E. J. *Chem. Rev.* **2006**, *106* (7), 2794–2810.
(18) Box, G. E. P.; Hill, W. J. *Technometrics* **1967**, *9* (1), 57–71.
(19) Blau, G.; Lasinski, M.; Orcun, S.; Hsu, S.-H.; Caruthers, J.; Delgass, N.; Venkatasubramanian, V. *Comput. Chem. Eng.* **2008**, *32* (4−5), 971–989.
(20) Hill, P. D. H. *Technometrics* **1978**, *20* (1), 15–21.
(21) Franceschini, G.; Macchietto, S. *Chem. Eng. Sci.* **2008**, *63* (19), 4846–4872.
(22) Asprey, S. P.; Macchietto, S. *Comput. Chem. Eng.* **2000**, *24* (2−7), 1261–1267.
(23) Ucinski, D.; Bogacka, B. T-Optimum designs for multiresponse dynamic heteroscedastic models. In *Moda 7: Advances in Model-Oriented Design and Analysis, Proceedings*; DiBucchianico, A., Lauter, H., Wynn, H. P., Eds.; Physica-Verlag GmbH & Co: Heidelberg, 2004; pp 191−199.
(24) Buzzi-Ferraris, G.; Forzatti, P. *Chem. Eng. Sci.* **1983**, *38* (2), 225–232.
(25) Schwaab, M.; Silva, F. M.; Queipo, C. A.; Barreto, J. A. G.; Nele, M.; Pinto, J. C. *Chem. Eng. Sci.* **2006**, *61* (17), 5791–5806.
(26) Buzzi Ferraris, G.; Forzatti, P.; Emig, G.; Hofmann, H. *Chem. Eng. Sci.* **1984**, *39* (1), 81–85.
(27) Buzzi-Ferraris, G.; Forzatti, P.; Paolo, C. *Chem. Eng. Sci.* **1990**, *45* (2), 477–481.
(28) Stewart, W. E.; Shon, Y.; Box, G. E. P. *AIChE J.* **1998**, *44* (6), 1404–1412.
(29) Espie, D.; Macchietto, S. *AIChE J.* **1989**, *35* (2), 223–229.
(30) Lacey, L.; Dunne, A. *J. Pharmacokinet. Pharmacodyn.* **1984**, *12* (3), 351–365.
(31) Hsu, S. H.; Stamatis, S. D.; Caruthers, J. M.; Delgass, W. N.; Venkatasubramanian, V.; Blau, G. E.; Lasinski, M.; Orcun, S. *Ind. Eng. Chem. Res.* **2009**, *48* (10), 4768–4790.
(32) Wiechert, W. *J. Biotechnol.* **2002**, *94* (1), 37–63.
(33) Burke, A. L.; Duever, T. A.; Penlidis, A. *Can. J. Chem. Eng.* **1997**, *75* (2), 422–436.
(34) Kamenski, D. I.; Dimitrov, S. D.; Silchenko, L. A.; Shestakov, G. K.; Odinzov, K. U.; Temkin, O. N. *Appl. Catal.* **1990**, *67* (1), 159–168.
(35) Farrell, R. J.; Tsai, Y. C. *AIChE J.* **1994**, *40* (4), 586–593.
(36) Froment, G. F. *AIChE J.* **1975**, *21* (6), 1041–1057.
(37) Greiner, L.; Ternbach, M. B. *Adv. Synth. Catal.* **2004**, *346* (11), 1392–1396.
(38) Chen, B. H.; Bermingham, S.; Neumann, A. H.; Kramer, H. J. M.; Asprey, S. P. *Ind. Eng. Chem. Res.* **2004**, *43* (16), 4889–4902.
(39) Issanchou, S.; Cognet, P.; Cabassud, M. *AIChE J.* **2005**, *51* (6), 1773–1781.
(40) Felix Oliver Lindner, P.; Hitzmann, B. *J. Theory Biol.* **2006**, *238* (1), 111–123.
(41) Fujiwara, M.; Nagy, Z. K.; Chew, J. W.; Braatz, R. D. *J. Process Control* **2005**, *15* (5), 493–504.
(42) Dantas, L. B.; Orlande, H. R. B.; Cotta, R. M. *Int. J. Therm. Sci.* **2002**, *41* (3), 217–227.
(43) Dewar, M. J. S.; Pyron, R. S. *J. Am. Chem. Soc.* **1970**, *92* (10), 3098–3103.
(44) Hoffmann, W.; Kang, Y.; Mitchell, J. C.; Snowden, M. J. *Org. Process Res. Dev.* **2007**, *11* (1), 25–29.
(45) Hartman, R. L.; Naber, J. R.; Zaborenko, N.; Buchwald, S. L.; Jensen, K. F. *Org. Process Res. Dev.* **2010**, *14* (6), 1347–1357.

(46) Leung, S.-A.; Winkle, R. F.; Wootton, R. C. R.; deMello, A. J. *Analyst* **2005**, *130* (1), 46–51.
(47) Chan, K. L. A.; Gulati, S.; Edel, J. B.; Mello, A. J. d.; Kazarian, S. G. *Lab Chip* **2009**, *9* (20), 2909–2913.
(48) Montgomery, D. C. *Design and Analysis of Experiments*; John Wiley: New York, 2001.
(49) Trachsel, F.; Gunther, A.; Khan, S.; Jensen, K. F. *Chem. Eng. Sci.* **2005**, *60* (21), 5729–5737.
(50) Barthe, P.; Guermeur, C.; Lobet, O.; Moreno, M.; Woehl, P.; Roberge, D. M.; Bieler, N.; Zimmermann, B. *Chem. Eng. Technol.* **2008**, *31* (8), 1146–1154.
(51) Lavric, E. D. Thermal Performance of Corning Glass Microstructures. In *ECI International Conference on Heat Transfer and Fluid Flow in Microscale*; Whistler: Canada, 2008.